

## Behavior of circular CFT columns subject to axial force and bending moment

Ji-Hyun Kwak<sup>1</sup>, Hyo-Gyoung Kwak<sup>1\*</sup> and Jin-Kook Kim<sup>2</sup>

<sup>1</sup>Civil and Environmental Engineering, Korea Advanced Institute of Science and Technology, Yuseong, Daejeon 305-701, Korea

<sup>2</sup>Steel Structure Research Division, Research Institute of Industrial Science and Technology, Yeonsu, Incheon 406-840, Korea

(Received December 13, 2012, Revised January 15, 2013, Accepted February 05, 2013)

**Abstract.** The major objective of this paper is to evaluate the behavior and ultimate resisting capacity of circular CFT columns. To consider the confinement effect, proper material models with respect to the confinement pressure are selected. A fiber section approach is adopted to simulate the nonlinear stress distribution along the section depth. Material nonlinearity due to the cracking of concrete and the yielding of the surrounding steel tube, as well as geometric nonlinearity due to the P- $\Delta$  effect, are taken into account. The validity of the proposed numerical analysis model is established by comparing the analytical predictions with the results from previous experimental studies about pure bending and eccentric axial loading. Numerical predictions using an unconfined material model were also compared to investigate the confinement effects on various loading combinations. The ultimate resisting capacities predicted by the proposed numerical model and the design guidelines in Eurocode 4 are compared to evaluate the existing design recommendation.

**Keywords:** circular CFT; confinement effect; ultimate resisting capacity; nonlinear FEM; short column

---

### 1. Introduction

A concrete-filled steel tube (henceforth simply CFT) is a beam-column member with a round or rectangular steel pipe in-filled with concrete to avoid local buckling. Due to the beneficial effects of the steel tube and the inner concrete, this type of a structure exhibits improved performance in terms of its flexibility, strength and energy absorption capacity. As the demand for seismic performance and space efficiency has increased in high-rise or mid-rise buildings over the past few recent decades, CFT is a good alternative to conventional RC members. The enhanced performances levels of CFT are mainly due to the confinement effect of concrete filling the hollow tube and restraining the steel tube against local buckling. However, a strength enhancement of CFT cannot be expected when the column section is rectangular (Hajjar *et al.* 1996, and Susantha *et al.* 2001) or the length of the column is long (Lakshmi *et al.* 2002, Huang *et al.* 2012). In contrast, experimental studies of a circular CFT short column present a noticeable strength

---

\*Corresponding author, Professor, E-mail: khg@kaist.ac.kr

increment (Schneider 1998, O'Shea *et al.* 2000, Sakino *et al.* 2004). Moreover, numerous confinement models for circular CFT have been developed on the basis of calibration from analytical results with experimental observations (Susantha *et al.* 2001, Hu *et al.* 2003, Sakino *et al.* 2004, Hu *et al.* 2010). Due to the discrepancies in those models, the author introduced a new method to evaluate the confinement effect on an axially loaded circular CFT column (Kwak *et al.* 2012). On the other hand, a column is subjected to a combination of axial force and bending moment, which may be due to the end restraint arising from the monolithic placement of the floor beams and the columns or due to eccentricity from an imperfect alignment. Due to the combination of the axial force and the bending moment, the column section must be designed so as to ensure that the acting forces in a member exist inside the axial force-moment (P-M) interaction diagram representing the resisting capacity of the column. O'Shea *et al.* (1998) conducted the eccentric axial load testing of circular CFT columns. Experimental results were illustrated with the interaction curves based on the provisions in Eurocode 4 and a fiber section analysis using the actual material properties. It was concluded that circular steel tubes filled with medium-strength concrete up to 50MPa can be conservatively designed using the provisions in Eurocode 4, while the interaction curve should be determined analytically using the unconfined concrete stress-strain curve for eccentricities larger than  $D/20$ . Hatzigeorgiou (2008) developed a simple fiber model based on a section analysis of circular CFT columns under a combination of axial force and bending moment. Empirical expressions of the confinement effects are proposed and corresponding uniaxial stress-strain relationships are used to configure the P-M interaction curve. It was reported that the strength of the CFT columns is deteriorated by the slenderness effect despite the fact that they are short columns with slenderness ratios of less than 30 (Wang *et al.* 2004, Baig *et al.* 2006). Therefore, a conventional fiber section analysis, which is unable to consider the slenderness effect, tends to overestimate the ultimate resisting capacity of CFT columns.

In this study, the behavior and ultimate resisting capacities of circular CFT columns are investigated using a one-dimensional fiber beam finite element model. To take into account the confinement effect in the CFT, the stress-strain relationships of both the concrete and the steel tube are proposed according to previous observations of CFT under axial compression. The geometric nonlinearity due to the  $P - \Delta$  effect is also considered to assess the structural behavior. The proposed numerical analysis model is validated through comparisons of the experimental results with various load combinations. These load combinations include 1) pure bending, 2) eccentric compression, and 3) a combination of axial force and bending moment. The effect of the proposed confinement model on both the behavior and the ultimate resisting capacity is also investigated in each case. Finally, the current design code for confined composite members is evaluated through comparisons with the analysis results.

## **2. Material model**

### *2.1 Concrete*

The response of a CFT structure sharply depends on the stress-strain relationship of the constituent materials and on the magnitude of the stress. When concrete is subjected to lateral confinement pressure, the strength and ductility, which are represented by the uniaxial compressive strength  $f'_{cc}$  and the corresponding strain  $\epsilon_{cc}$ , are much higher than those of

unconfined concrete. On the basis of experimental observations, Richart *et al.*(1928) revealed that the increment of the strength and ductility is proportional to the confinement pressure. This linear relationship tends to overestimate the strength of confined concrete when the confinement pressure is high. Later, Mander *et al.*(1988) suggested the following equations to represent the relationships for those values between confined and unconfined concrete

$$f'_{cc} = f'_c \left( -1.254 + 2.254 \sqrt{1 + 7.94 \frac{\sigma_r}{f'_c} - 2 \frac{\sigma_r}{f'_c}} \right) \quad (1)$$

$$\varepsilon_{cc} = \varepsilon_{c0} \left[ 1 + 5 \left( \frac{f'_{cc}}{f'_c} - 1 \right) \right] \quad (2)$$

where  $\sigma_r$  is the confinement pressure, and  $f'_c$  and  $\varepsilon_{c0}$  are the strength and the corresponding strain of unconfined concrete. The confinement pressure  $\sigma_r$  is determined from the force equilibrium equation at a CFT section. It is expressed by the relationship of  $\sigma_r = 2t\sigma_\theta / (D-2t)$ , where  $\sigma_\theta$  is the hoop stress,  $t$  is the thickness and  $D$  is the diameter of the steel tube. Due to the simplicity and accuracy, this model is widely used in numerical analyses on CFT including this study (Elremaily *et al.* 2002, Fam *et al.* 2004, Liang *et al.* 2009).

The uniaxial stress-strain relationship during compression is described using three regions (see Fig. 1 (a)). When the concrete strain  $\varepsilon_c$  is less than  $\varepsilon_{cc}$ , the monotonic envelope curve introduced by Mander *et al.* (1988) is adopted in this paper. It maintains an initial modulus regardless of the strength enhancement due to confinement and has the following form

$$\sigma_c = f'_{cc} \frac{x\gamma}{\gamma - 1 + x^\gamma} \quad (3)$$

Here,  $\sigma_c$  is the stress of concrete corresponding to the strain of concrete  $\varepsilon_c$ ,  $\gamma = E_c / (E_c - f'_{cc} / \varepsilon_{cc})$ , and  $x = \varepsilon_c / \varepsilon_{cc}$ .  $E_c$  is modulus of elasticity of concrete. The softening behavior, when  $\varepsilon_c$  is greater than  $\varepsilon_{cc}$ , is assumed to be linearly descending. Finally it is assumed that the concrete is unable to resist any stress after the ultimate strain  $\varepsilon_{cu}$ .

The tension region of concrete is assumed to be linear elastic. Beyond the tensile strength, the tensile stress decreases linearly (see Fig. 1(b)). The ultimate tensile failure from cracking is assumed to occur when the principal tensile strain exceeds the value  $\varepsilon_{ut} = 2G_f / f_t \ln(3/b) / (3-b)$ .

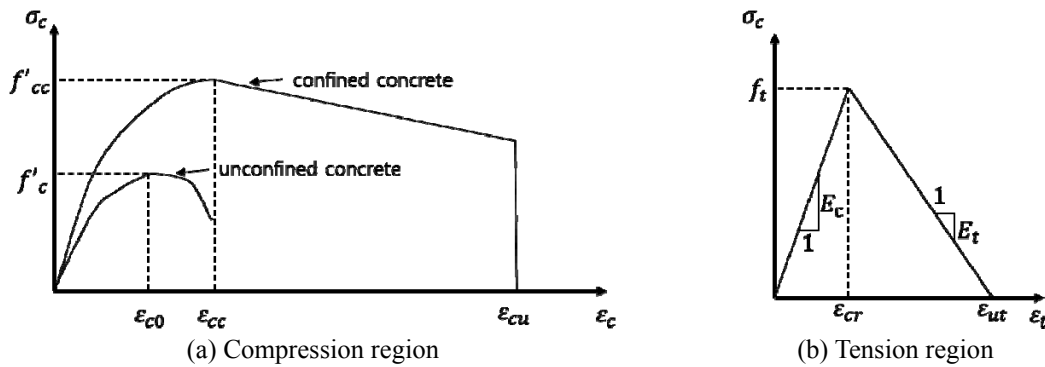


Fig. 1 Stress-strain relationship of concrete

In this equation,  $b$  denotes the element length used in the finite element analysis and  $G_f$  is the fracture energy that is dissipated during the formation of a crack in the unit length per unit thickness. This is considered to be a material property. The value of  $\varepsilon_{ut}$  is derived from the fracture mechanics concept by equating the crack energy release with the fracture toughness of concrete  $G_f$  (Kwak *et al.* 1990).

## 2.2 Steel

The stress-strain relationship for a steel tube is assumed to be linear elastic-perfect plastic with an elastic modulus  $E_s$  of 200GPa. When the stress exceeds the yield stress  $f_y$ , the steel tube will exhibit plastic deformation. Because a steel tube is usually subjected to biaxial stresses in CFT, a von Mises yield criterion  $F$  is employed to define the elastic limit, which is written as

$$F = \sqrt{3J_2} = \sqrt{(\sigma_{1s} - \sigma_\theta)^2 + \sigma_{1s}^2 + \sigma_\theta^2} / \sqrt{2} = f_y \quad (4)$$

where  $J_2$  denotes the second stress invariant of the stress deviator tensor,  $\sigma_{1s}$  is the longitudinal stress and  $\sigma_\theta$  is the transverse (hoop) stress. Once maximum hoop stress is determined using Eq.(12), the longitudinal yield stresses of the steel tube characterized by different yield stresses of tension  $f_{yt}$ , and the compression  $f_{yc}$  are given by

$$f_{yt} = 0.5 \left( \sigma_\theta + \sqrt{4f_y^2 - 3\sigma_\theta^2} \right), \quad f_{yc} = 0.5 \left( \sigma_\theta - \sqrt{4f_y^2 - 3\sigma_\theta^2} \right) \quad (5)$$

## 3. Determination of confinement effect

Knowledge of confinement pressure is essential because it strongly affects the behavior and strength not only of the steel tube but also of concrete core (see Eqs. (1) and (5)). To obtain the maximum confinement pressure of CFT subjected to axial compression, the relationships between the stress and strain components of the constitutive materials are induced. A combination of axial compression and confinement pressure causes tri-axial stress in concrete. The increments in the stress and strains of concrete in the longitudinal direction are denoted as  $\Delta\sigma_{1c}$  and  $\Delta\varepsilon_{1c}$  (see Fig. 2(a)). Those values in the transverse direction are  $\Delta\sigma_{rc}$  and  $\Delta\varepsilon_{rc}$ . Thus, the stress-strain relationships according to the Hooke's law become

$$\Delta\varepsilon_{1c} = \frac{\Delta\sigma_{1c}}{E_c} - 2\nu_c \frac{\Delta\sigma_{rc}}{E_c} \quad (6)$$

$$\Delta\varepsilon_{rc} = (1 - \nu_c) \frac{\Delta\sigma_{rc}}{E_c} - \nu_c \frac{\Delta\sigma_{1c}}{E_c} \quad (7)$$

The stresses of a compressed steel tube in CFT consist of longitudinal compression and hoop tension. The longitudinal stress and strain increment are denoted as  $\Delta\sigma_{1s}$  and  $\Delta\varepsilon_{1s}$ , and hoop stress and strain are denoted as  $\Delta\sigma_{\theta s}$  and  $\Delta\varepsilon_{\theta s}$  (see Fig. 2(b)). The stress and strain relationships in a biaxially stressed steel tube are

$$\Delta \varepsilon_{1s} = \frac{1}{E_s} (\Delta \sigma_{1s} - \nu_s \Delta \sigma_{\theta s}) \quad (8)$$

$$\Delta \varepsilon_{\theta s} = \frac{1}{E_s} (\Delta \sigma_{\theta s} - \nu_s \Delta \sigma_{1s}) \quad (9)$$

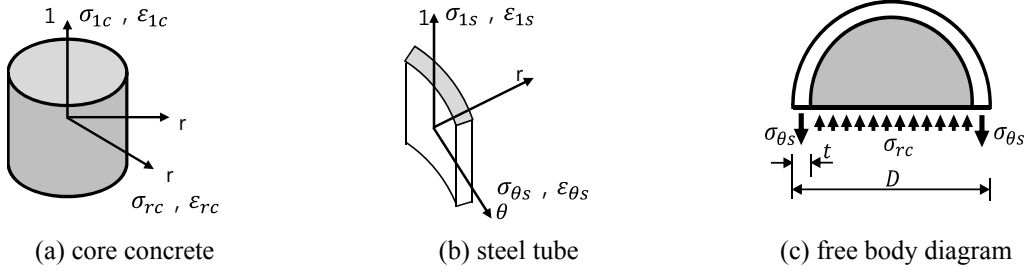


Fig. 2 Stress and strain components of constitutive material

The confinement pressure on concrete is compressive and the hoop stress of the steel is tensile because the surrounding steel resists the expansion of the core concrete. The relationship between the confinement pressure and the hoop stress can be determined from the equilibrium of the forces acting on the free body diagram (Fig. 2(c)), as follows

$$2t\Delta\sigma_{\theta s} + (D-2t)\Delta\sigma_{rc} = 0 \quad (10)$$

Both the longitudinal and transverse strains of concrete and the steel tube are equal to each other under the assumption of a perfect bond between the two materials. This compatibility condition leads to  $\Delta\varepsilon_{1c} = \Delta\varepsilon_{1s}$  and  $\Delta\varepsilon_{rc} = \Delta\varepsilon_{\theta}$ . Simultaneously solving the stress-strain relationship, the force equilibrium equation and compatibility condition gives the following relationship

$$\Delta\varepsilon_{1c} = \frac{1}{\nu_c - \nu_s} \left\{ (1 - \nu_c - 2\nu_c^2) \frac{\Delta\varepsilon_{rc}}{E_c} + \frac{(D-2t)}{2tE_s} (1 - \nu_s^2) \Delta\sigma_{rc} \right\} \quad (11)$$

The above equation contains nonlinear properties of the concrete, in this case the Poisson's ratio and the stress-strain relationship; thus, an incremental iterative numerical procedure is required to solve it. In addition, the maximum confinement stress can be obtained using the von-Mises yield criteria, as the yielded steel tube fails to provide additional confinement to the inner concrete. According to numerical research on the stress components in CFT subjected to axial loading conducted by Kwak *et al.* (2012), the maximum hoop stress can be simply estimated in terms of the yield strength of a steel tube  $f_y$  as  $\sigma_{\theta,max} = \alpha f_y$ , where the coefficient  $\alpha$  is defined as follows

$$0 \leq \alpha = 8.77 \times 10^{-6} f_y^2 - 2.47 \times 10^{-3} f_y + 0.13 \leq 0.206 \quad (12)$$

Once  $\alpha$  is determined, the maximum hoop stress ( $\sigma_{\theta,max} = \alpha f_y$ ), maximum confinement stress ( $\sigma_{rc}$  in Eq.(10)), the strength of the confined concrete ( $f'_{cc}$  in Eq.(1)) and the longitudinal yield strength of the steel tube ( $f_{yt}$  and  $f_{yc}$  in Eq.(5)) can be calculated sequentially. To evaluate the

confinement effect on the structural behavior of a circular CFT, the modified material properties from the above equations are used in the following finite element procedure.

#### 4. Solution algorithm

To analyze the CFT columns, a layered section approach based on the Euler beam theory was employed in this study. This approach and the beam theory are both well established and widely used in analyses of beams. Additional details pertaining to the formulation of the beam elements can be found in the literature (Kwak *et al.* 2010). In a typical Euler beam, it is common to assume that plane sections remain planar to represent the linearity in the strain distribution of any section at any loading history. As the global stiffness matrix of the structure depends on the displacement increments, the solution of the equilibrium equations is typically accomplished by an iterative method through a convergence check. The nonlinear solution scheme selected in this study uses an arc-length method to observe the post-peak behavior; that is, an incremental-iterative method is used. All of the remaining algorithms, from the construction of an element stiffness matrix to the iteration at each load step, are shown in Fig. 3.

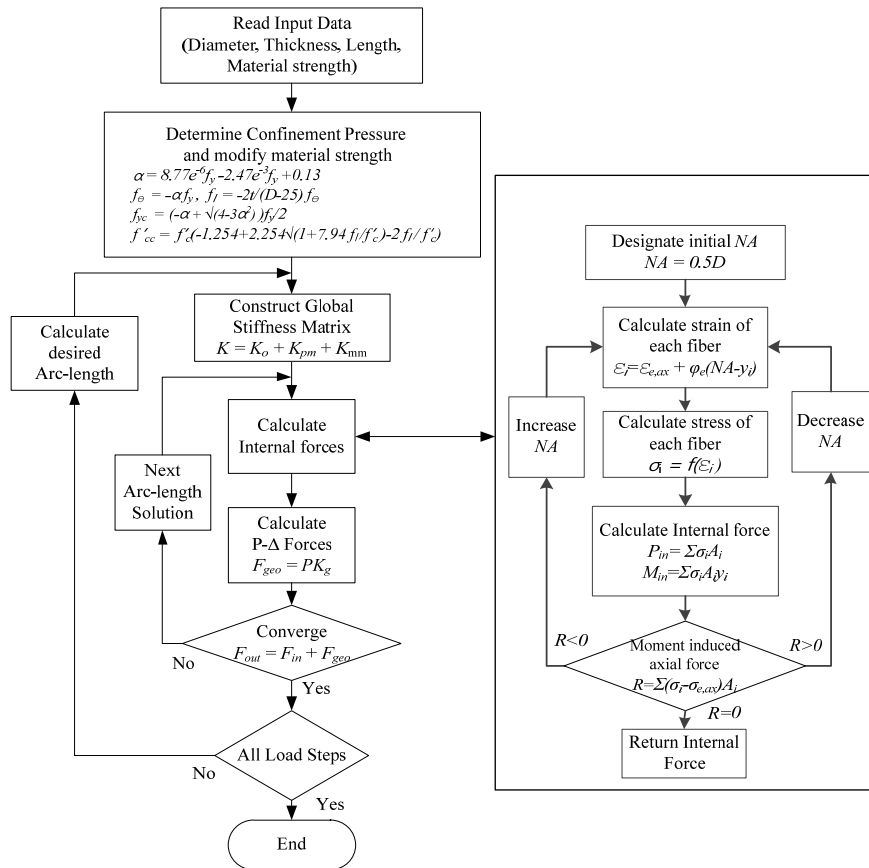


Fig. 3 Nonlinear finite element procedure

## 5. Verification

The experimental results are used to verify the numerical analysis model proposed in this paper. Load combinations of each experimental set up in this section are carefully selected to verify the accuracy of the proposed model. A total of three distinct cases of load combinations are selected. These are 1) pure bending, 2) eccentric compression, and 3) fixed axial loading with a gradual increase in the bending moment. The behaviors of each CFT column are investigated through the moment-curvature relationships or by the ultimate axial loads. In addition, the ultimate resisting capacities of a series of test specimens with equal geometric and material properties with various eccentricities facilitate the determination of the axial load and the bending moment interaction diagram.

### 5.1 Pure bending

Direct application of the proposed confinement model for concrete may be inappropriate for a pure bending problem because the distribution of the confinement pressure is nonlinear along the section depth (see Fig. 4). Therefore, the uniaxial strength of each layer in a concrete section is different and the stress-strain relationship of each layer should also be uniquely defined. However, more than half of the concrete layer is in the tension region, and the slope of the softening branch of the confined compressive concrete is moderate. Thus, it can be expected that the proposed FE model, a relatively simplified 1D beam analysis, can successfully evaluate the macro behavior of a CFT column.



Fig. 4 Typical transverse stress distribution of confined concrete under a pure bending condition

Elchalakani *et al.* (2001) used a unique pure bending rig to obtain the behavior of a circular CFT under pure bending moment. The advantage of this rig is its ability to apply a pure bending moment condition over the middle span of a test specimen without inducing significant axial or shear forces. The moment-curvature relationships between four typical specimens are illustrated in Fig. 5. Additionally, numerical results using unconfined material properties were conducted to investigate the confinement effects on the pure bending behavior of a circular CFT. Detailed properties of the test specimens and the measured ultimate moments from the experimental and numerical investigations are given in Table 1. The depth-to-thickness ratios of the test specimens generally range from 12.8 to 40.2, as achieved by reducing the diameter from 101.83mm to 33.78mm. The yield strengths of the steel tubes range from 365MPa to 460MPa, while the unconfined compressive strength of concrete is consistent at 23.4MPa.

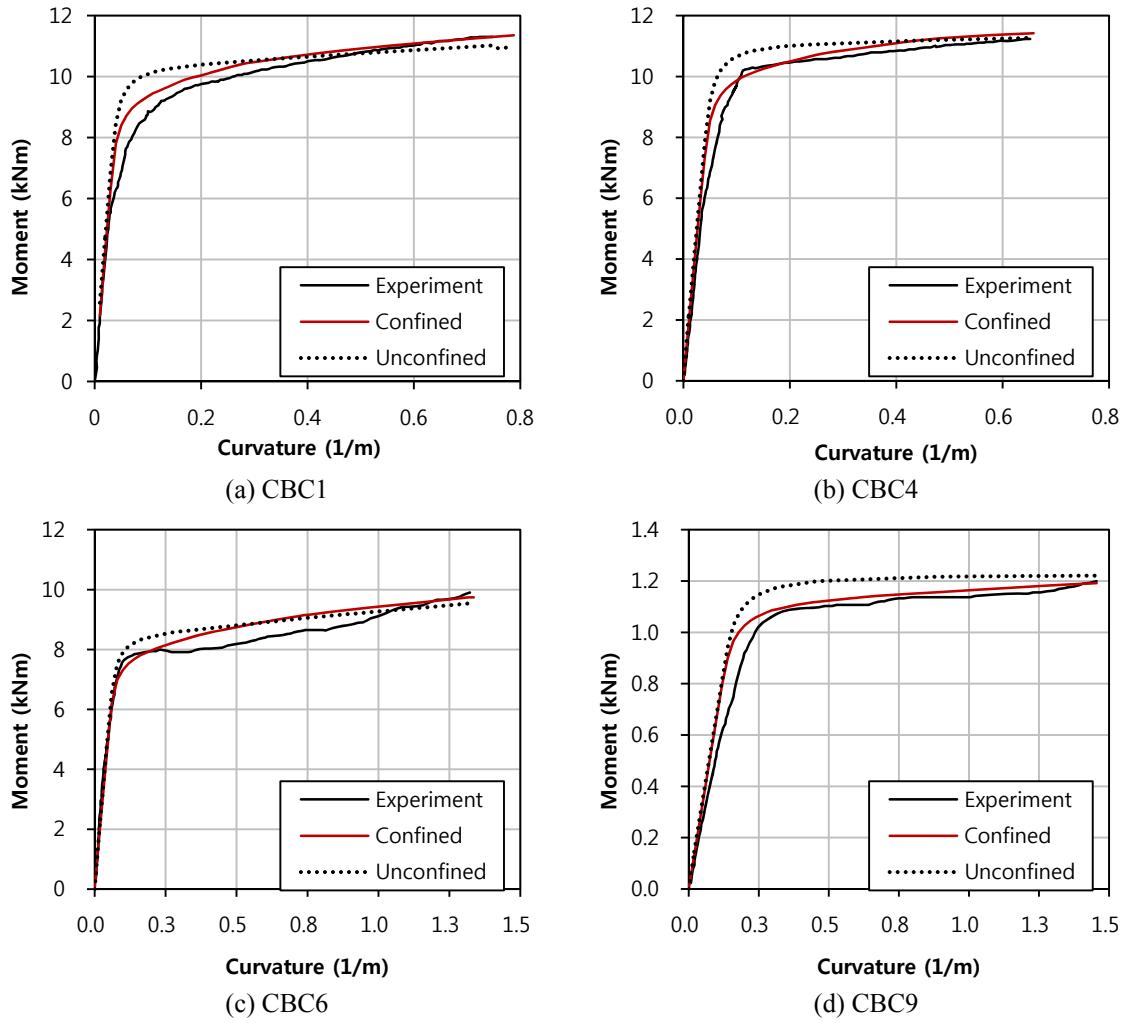


Fig. 5 Moment curvature relationships of pure bending specimens

Table 1 Properties of pure bending specimens

specimen	$D$ (mm)	$t$ (mm)	$D/t$	$f_y$ (MPa)	$f'_c$ (MPa)	$E_s$ (GPa)	$M_{u,exp}$ (kN-m)	$M_{u,conf}$ (kN-m)	$M_{u,unconf}$ (kN-m)
<b>CBC1</b>	101.83	2.53	40.2	365	23.4	200	11.03	11.35	11.02
<b>CBC2</b>	88.64	2.79	31.8	432	23.4	210	10.96	11.02	10.89
<b>CBC3</b>	76.32	2.45	31.2	415	23.4	218	6.82	6.84	6.72
<b>CBC4</b>	89.26	3.35	26.6	412	23.4	211	11.23	11.42	11.27
<b>CBC5</b>	60.65	2.44	24.9	433	23.4	211	3.97	4.02	3.96
<b>CBC6</b>	76.19	3.24	23.5	456	23.4	205	9.90	9.74	9.55
<b>CBC7</b>	60.67	3.01	20.2	408	23.4	204	4.99	4.80	4.72
<b>CBC8</b>	33.66	1.98	17	442	23.4	207	0.92	0.93	0.93
<b>CBC9</b>	33.78	2.63	12.8	460	23.4	209	1.20	1.19	1.22

It can be observed in Fig. 5 that both the confined and the unconfined material models successfully estimate the ultimate bending moment of CFT under pure bending. Therefore, the ultimate moment is not affected by the confinement effect. That is, the strength enhancement of CFT cannot normally be expected in a pure bending condition. The design guideline in the Eurocode 4 (2004) suggests that the resistance of the cross-section may be calculated while assuming rectangular stress blocks. Moreover, the reduction factor can be ignored, especially for concrete-filled sections. An analytical investigation of Fig. 5 supports this guideline. On the other hand, it is also observed that the results of the confined model exhibit much more flexible behavior compared to that of the unconfined model. Hence, to avoid an overestimation of the stiffness, a rigorous analysis considering the confinement effect may be inevitable to design CFT as a beam member.

## 5.2 Eccentric axial loading

Eccentric compression combines compression and bending. 16 columns under eccentric axial loading are examined from O'shea and Bridge (1998), for which Table 2 presents the dimensions and the material properties. This table also presents the combined compression and bending capacity values for these columns as predicted numerically by the proposed method and experiments. The test specimens have a large variety of  $D/t$  ratios, axial compressive strengths of concrete and yield strengths of steel tubes. The different eccentricities have various combinations of axial loading and bending moment proportions.

Fig. 6 illustrates the ratios between capacities of these CFT short columns and the predictions of the numerical model. Those ratios in Eurocode 4 predictions are also plotted. As shown in Fig. 6, it is clear that the numerical results obtained from this study are in excellent agreement with those obtained from the experiment, thus confirming the validity of the proposed model. Therefore, the proposed method demonstrates very good analytical predictions of the ultimate strength levels of CFT. In this experimental set up, the eccentricities are mainly less than  $0.1D$ ; thus, the following prediction formula for the axial governing region in Eurocode 4 was applied

$$N_{pl,Rd} = \eta_a A_a f_{yd} + A_c f_{cd} \left( 1 + \eta_c \frac{t}{D} \frac{f_y}{f_{ck}} \right) \quad (13)$$

Here,  $\eta_a = \eta_{a0} + (1 - \eta_{a0})(10e/D)$  and  $\eta_c = \eta_{c0}(1 - 10e/D)$ . In addition, Fig. 6 shows that the predictions by Eurocode 4 significantly overestimate the ultimate axial strength of CFT. Therefore, an estimation using Eurocode 4 with a small amount of eccentricity is dangerous and a modification is required.

An interaction curve for the axial force and the bending moment can be obtained by a series of experiments with various eccentricities. These experiments for a circular CFT were conducted by Furlong (1967). The diameter of the specimen is 127mm, the thickness is 2.41mm,  $f'_c$  is 35MPa,  $f_y$  is 280MPa and the slenderness ratio  $kl/r$  is 26.02. The ultimate resisting capacities from the experimental results, predicted by Eurocode 4, the numerical model using a confined model and that using an unconfined model are illustrated in Fig. 7.

Table 2 Properties and ultimate strength of eccentric compression specimens

No.	Specimen	$D$ (mm)	$t$ (mm)	$L$ (mm)	$f'_c$ (MPa)	$f_f$ (MPa)	$E_s$ (MPa)	$e$ (mm)	$P_{exp}$ (kN)	$P_{anal}$ (kN)
1	S30E250B	165	2.82	580.5	48.3	363.3	200,588	7.0	1,525	1,268
2	S20E250A	190	1.94	661.0	41.0	256.4	204,686	8.6	1,533	1,281
3	S12E250A	190	1.13	663.5	41.0	185.7	178,366	8.5	1,229	1,060
4	S10E250A	190	0.86	662.0	41.0	210.7	177,035	7.4	1,219	1,104
5	S30E150B	165	2.82	580.0	48.3	363.3	200,588	17.2	1,123	912
6	S20E150A	190	1.94	664.0	41.0	256.4	204,686	16.2	1,284	1,216
7	S16E150B	190	1.52	662.0	48.3	306.1	207,403	15.5	1,260	1,211
8	S12E150A	190	1.13	664.0	41.0	185.7	178,366	18.9	1,023	1,026
9	S10E150A	190	0.86	663.0	41.0	210.7	177,035	13.9	1,017	1,005
10	S30E280A	165	2.82	579.5	80.2	363.3	200,588	9.4	1,940	1,573
11	S20E280B	190	1.94	662.5	74.7	256.4	204,686	10.0	2,203	1,931
12	S10E280B	190	0.86	665.5	74.7	210.7	177,035	8.6	1,910	1,780
13	S30E180A	165	2.82	579.5	80.2	363.3	200,588	17.9	1,653	1,173
14	S20E180B	190	1.94	663.0	74.7	256.4	204,686	20.8	1,730	1,866
15	S16E180A	190	1.52	663.5	80.2	306.1	207,403	14.3	1,925	1,683
16	S10E180B	190	0.86	665.0	74.7	210.7	177,035	17.9	1,532	1,732

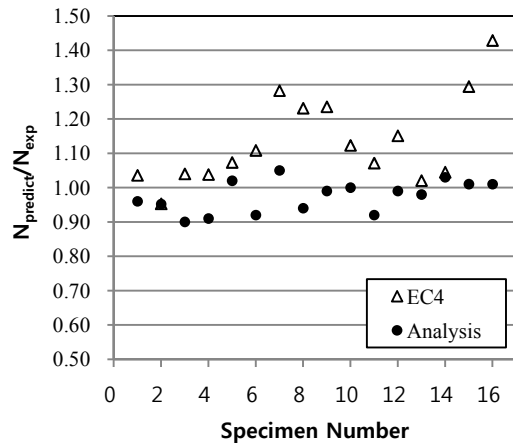


Fig. 6 Comparison of ultimate strengths subjected to eccentric compression

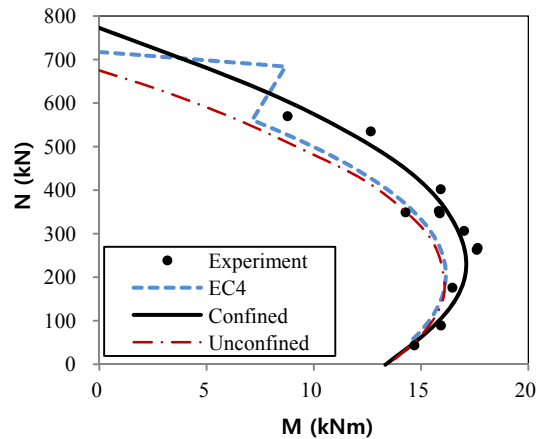


Fig. 7 Interaction curves for eccentric compression

The interaction curve predicted by the numerical analysis considering the confinement effect is best fit to the experimental results. Also, the provisions in Eurocode 4, a simplified method, provide a reasonable estimation of the interaction curve. It should be noted that even an indirect consideration of the confinement effect by a rectangular stress block can successfully predict the ultimate resisting capacity of CFT. Fig. 7 shows that the resisting capacities of CFT predicted by the confined model and the unconfined model are nearly equivalent in a moment-dominant region.

Table 3 Properties of the combined axial force and moment specimens

Specimen	$N_{axial}$ (kN)	$D$ (mm)	$t$ (mm)	$L$ (mm)	$f_y$ (MPa)	$f'_c$ (MPa)	$M_{u,exp}$ (kN-m)	$M_{u,conf}$ (kN-m)	$M_{u,unconf}$ (kN-m)
CU0	0	280	4	1100	285	24.2	131	133	133
CU023	542	280	4	1100	285	24.2	155	155	137
CU034	812	280	4	1100	285	24.2	160	164	144
CU045	1200	280	4	1100	288	29.1	183	194	129
CU056	1354	280	4	1100	285	24.2	171	167	102
CU074	2000	280	4	1100	288	29.1	159	165	68

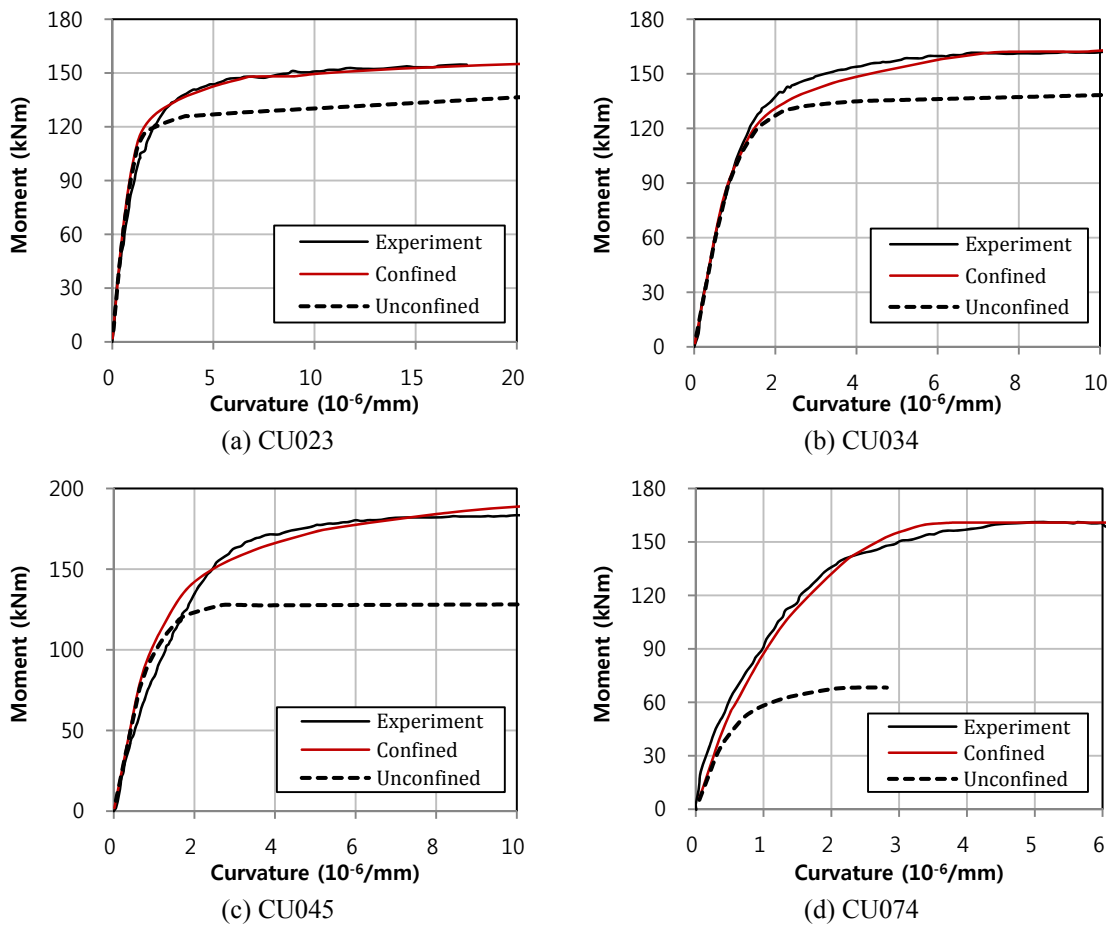


Fig. 8 Moment curvature relationship of combined axial force and bending specimens

This coincides with the pure bending cases. However, the unconfined model significantly underestimates the resisting capacity in an axial-force-dominant region despite the relatively low confinement pressure, even when a large  $D/t$  ratio of 52 is applied. For example, the predicted moment capacity at an axial force of 600kN using the unconfined model is roughly half that of the confined model.

### 5.3 Axial force and bending moment combination

Liu *et al.* (2003) conducted an experiment on CFT specimens subject to a combination of axial force and bending moment. In this experiment, an axial actuator supplies axial compression and lateral actuators provide two-point lateral loading onto a rigid body connected to each end of a CFT specimen. Therefore, the axial force and bending moment can be independently applied. In each test, a certain level of axial compression is initially applied and the bending moment is then gradually applied until failure. Therefore, the moment-curvature relationships under various axial load levels can be obtained. Detailed properties of seven test specimens are given in Table 3. Every specimen has the same dimensions, but specimens CU045 and CU075 are composed of concrete with slightly higher strengths compared to the others. The numbers in the specimen names denote the percentage of loaded axial force with respect to the ultimate axial strength of the section.

Comparisons of the moment-curvature relationships between the experimental and the numerical prediction using confined model and the unconfined model are illustrated in Fig. 8. The order of the plots is sorted by specimen name, which is equal to sorting by the applied axial force level. The results of the analysis are in good agreement with not only the predictions of the ultimate moment but also the nonlinear behavior of the CFT columns. Note that most of the analytical results slightly underestimate the overall moment-curvature behavior. That is, the results of the analytical model are on the safe side. Therefore, the proposed model may be successfully adopted for the design procedure without sacrificing any accuracy. The ultimate moments predicted by the unconfined model significantly decreased as the initial fixed axial force increased. This is in agreement with the interaction curves shown in Fig. 7, also confirming the importance of considering the confinement effect in numerical evaluations of the behavior of CFT columns.

## 6. Evaluation of the design recommendation

Eurocode 4 (2004) is the only design guideline for confined composite members considering the confinement effect. It provides the most accurate predictions of the ultimate resisting capacity (Giakoumelis *et al.* 2004). This code also considers the slenderness effect by adopting the relative slenderness  $\lambda$ , which is a function of the column length  $L$ , despite the fact that the limitation of  $\lambda < 0.5$  implies a short column. In addition, the axial compression and bending moment interaction curve is calculated using rectangular stress blocks, as shown in Fig. 9. The tensile strength of the concrete is typically neglected.

According to the above method, there is a discontinuity in the interaction curve (see the black solid line in Fig. 9). Moreover, previous overestimations of Eurocode 4 shown in Fig. 7 which shows eccentrically loaded cases with eccentricities less than or equivalent to  $0.1D$ , implying that the provision of Eurocode 4 in cases involving low eccentricity is not valid. Thus, the author suggests a slight modification in the form of a linear connection between  $N_{pl,Rd}$  for  $e=0$  and the point corresponding to  $e=0.1D$  at the stress-block-based interaction curve (see the gray solid line in Fig. 9). The axial force-bending moment interaction diagram represents the ultimate resisting capacity of the column member. As mentioned earlier, the provision in Eurocode 4 suggests that plastic resistance to a concentric axial load should take into account the slenderness ratio of the CFT column. Thus, the validity of Eq. (13) according to various slenderness ratios is investigated in a comparison with a 1D beam finite element analysis. The following material and geometric

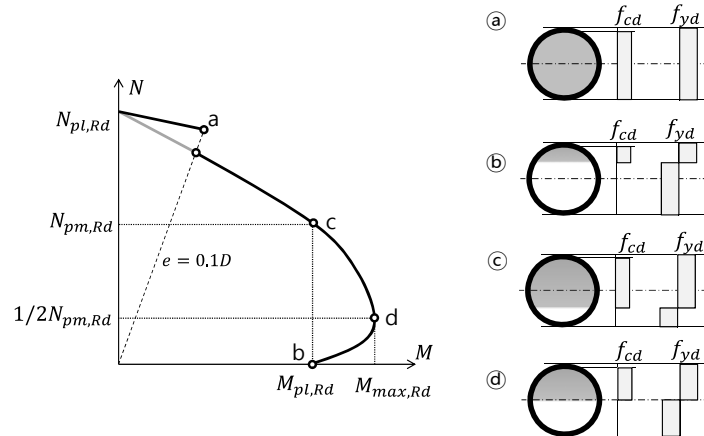


Fig. 9 Interaction curve and corresponding stress distribution in Eurocode 4

properties are assumed:  $E_s = 200$  GPa,  $f_y = 350$  MPa,  $f'_c = 35$  MPa,  $D = 300$  mm and  $t = 15$  mm. Three slenderness ratio values ( $kL/r = 10, 20$  and  $30$ ) are assessed. The slenderness ratio is limited to  $30$ , as the resisting capacity of columns with a slenderness ratio greater than  $30$  is seriously influenced by the  $P-\Delta$  effect (Kwak *et al.* 2010) and because slender columns do not exhibit the beneficial effects of composite behavior (Huang *et al.* 2012). The resulting interaction curves are illustrated in Fig. 10.

Fig. 10 shows that there are discrepancies between analysis result and prediction from the Eurocode 4 except for slenderness ratio  $30$ . Analysis result presents that the relatively long columns have less resisting capacity due to the  $P-\Delta$  effect. Therefore, Eurocode 4, which ignores the  $P-\Delta$  effect when  $e/D > 0.1$ , gives a conservative estimation. Moreover, a region in which the axial force is dominant, i.e.,  $e/D < 0.1$ , predictions of the Eurocode 4 seem to give underestimated values, except when the axial compressive strength at  $kL/r = 10$ .

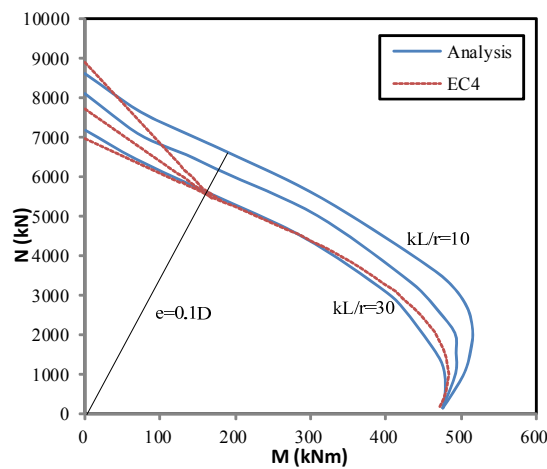


Fig. 10 CFT interaction curves in accordance with the slenderness ratio

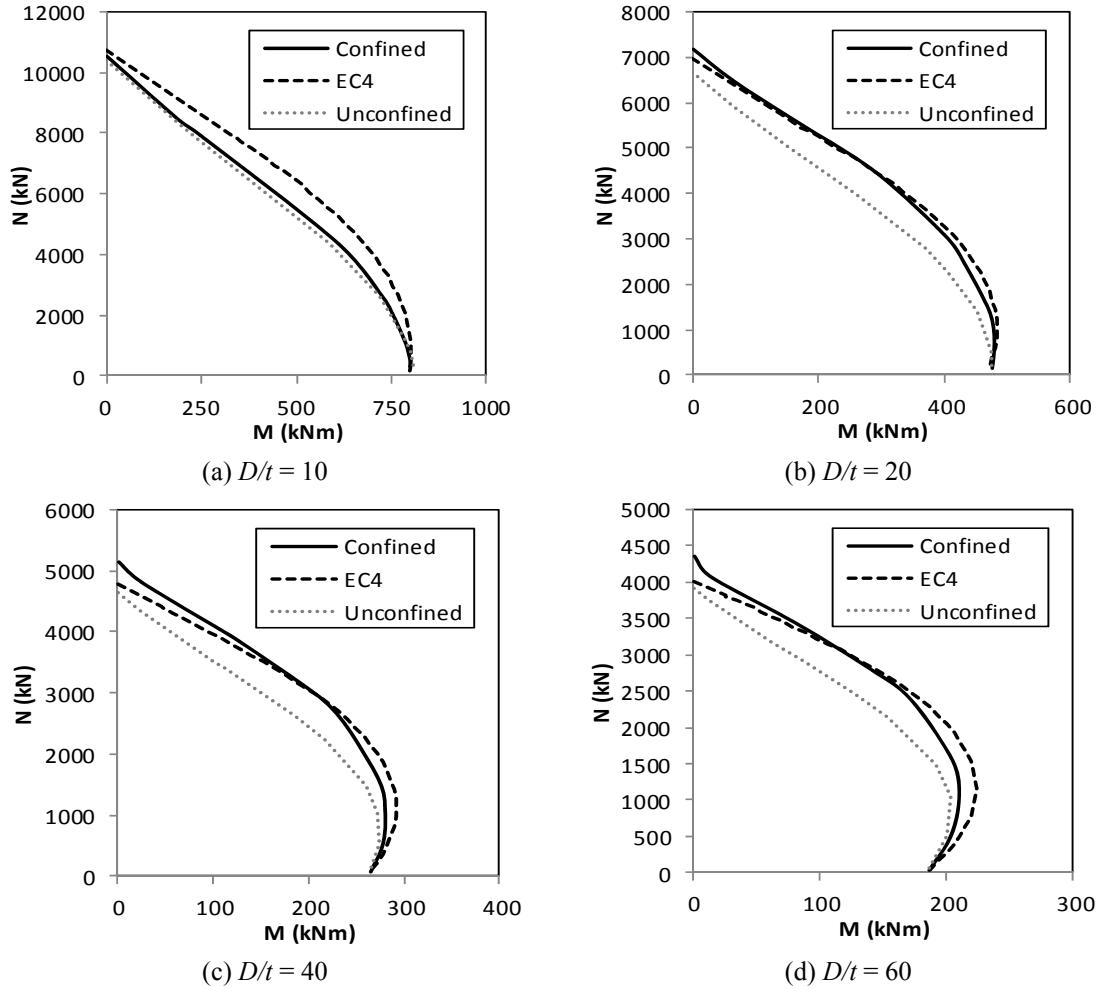


Fig. 11 Interaction diagrams of CFT in accordance with the  $D/t$  ratio

This can explain the overestimations of the axial resisting capacities of Eurocode 4 for the experimental specimens depicted in Fig. 6, as the slenderness ratios of the test specimens are commonly around 15. Considering that a column is an axial member and is usually exposed to small eccentricities, underestimation of the axial region may yield an uneconomical design. Thus, the assumption of full plasticity for a very short CFT column is inappropriate. However, predictions by Eurocode 4 are less than those obtained from the analyses in all of the investigated slenderness ratios. Hence, Eurocode 4 provides a safety estimation of the resisting capacity of a normal-strength CFT column.

Fig. 11 presents the ultimate resisting capacities of the CFT columns for various values of  $D/t$  ratios. The material properties assume a normal grade, in this case  $f_y = 350$  MPa and  $f'_c = 35$  MPa. The slenderness ratio is  $kL/r = 30$ , as previously mentioned, to ensure good agreement between Eurocode 4 and the numerical results. The diameters are fixed at 300mm and the thickness of the steel tube ranges from 5mm to 30mm in all cases, in accordance with the  $D/t$  ratios of 10, 20, 40

and 60. Eurocode 4 restricts the maximum values of the  $D/t$  ratio to  $D/t = 90 \times 235/f_y$ ; thus,  $D/t = 60.4$  is the maximum value for the 350MPa steel tube. Generally, Eurocode 4 provides a reasonable estimate of the interaction curve for the overall  $D/t$  range. A slight improvement of resisting capacity was observed when thick (30mm) steel tube is adopted(see Fig. 11(a)). This may be due to the fact that large confinement pressure deteriorate the longitudinal yield strength of steel tube as mentioned in previous study (Kwak *et al.* 2012).The ultimate resisting capacity variations due to yield strengths of the steel tubes are plotted in Fig. 12. The yield strengths of the steel tubes ranged from 250 MPa to 750 MPa, with  $f'_c = 35$  MPa,  $D = 300$ mm,  $t = 15$ mm and  $kL/r = 30$ . It should be noted that the confinement pressure is very low if a low-strength steel tube, such as the 250 MPa tube here, is used. In this case, the corresponding maximum hoop strength indicator  $\alpha$  is 0.06, which is less than 1/3 of the value of  $\alpha$  at 0.206 for a yield strength of more than 350MPa. Even with a small amount of confining pressure, analysis result exhibits very good agreement with Eurocode 4. It can be indirectly concluded that the relationship between the yield strength of concrete and the confinement effect is considerable for a relatively low-strength steel tube.

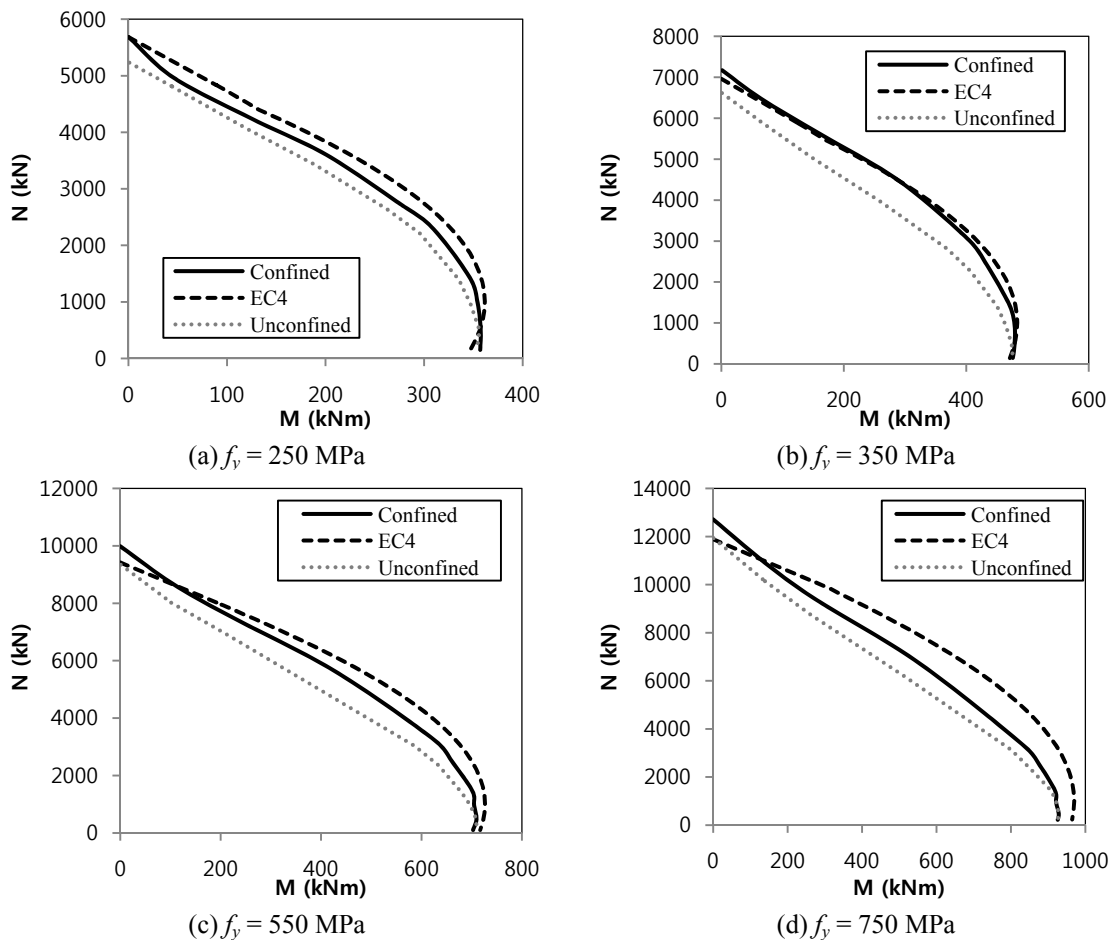


Fig. 12 Interaction diagrams of CFT in accordance with the strength of steel tube

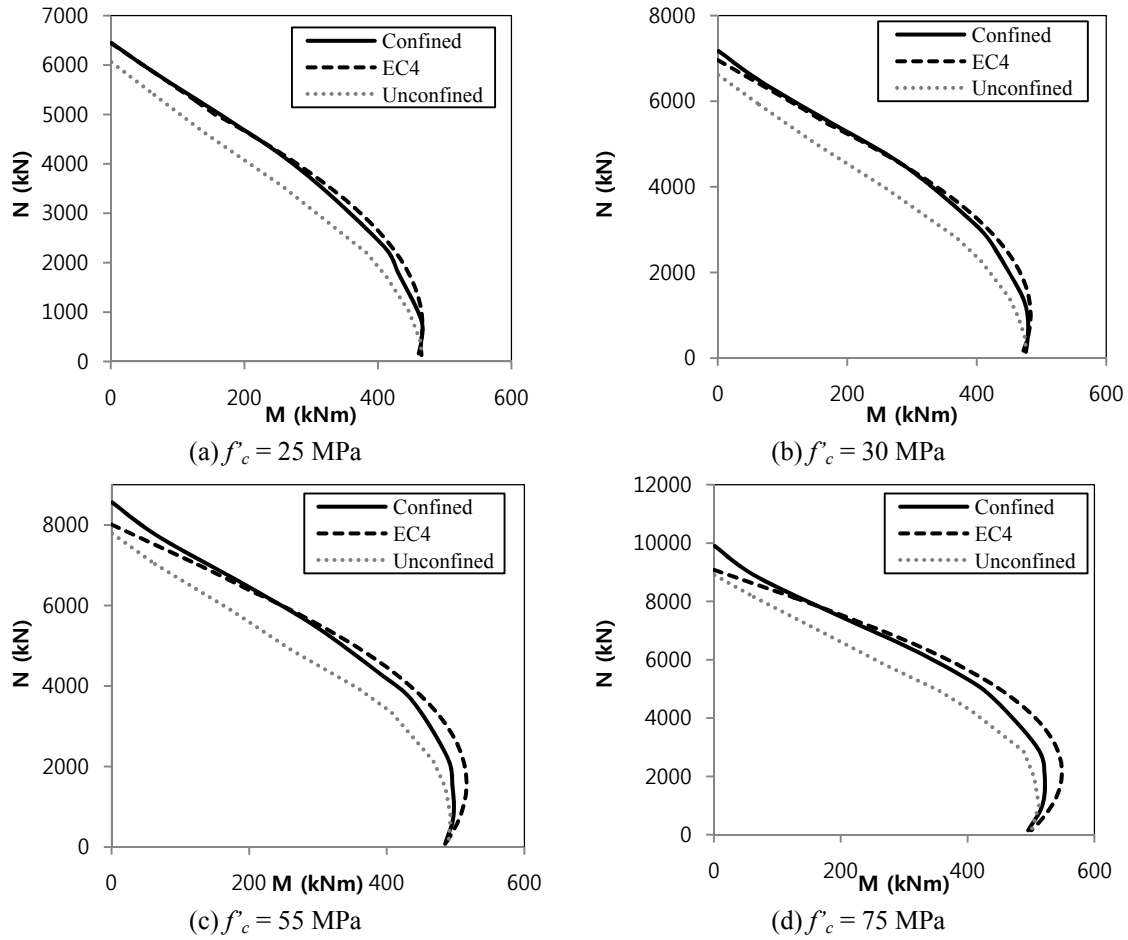


Fig. 13 Interaction diagrams of CFT in accordance with the strength of concrete

On the other hand, Eurocode 4 appears to non-conservatively predict the ultimate resisting capacity of a CFT column as the yield strength of the steel tube increases. The interaction curve becomes linear for a high-strength steel tube, such as the 750MPa tube here. In this case, the ratio of the load carried by the steel to entire the cross-section,  $A_s f_y / (A_s f_y + A_c f'_c)$ , is 0.85. Therefore, the behavior of the CFT column is governed by the steel tube. In addition, the difference between the confined model and the unconfined model is slight. Therefore, the combination of a high-strength steel tube and normal-strength concrete is not desirable.

Interaction diagrams with various strengths of concrete are shown in Fig. 13. The concrete strengths ranged from 25MPa to 75MPa, with  $f_y = 350\text{MPa}$ ,  $D = 300\text{mm}$ ,  $t = 15\text{mm}$  and  $kL/r = 30$ . It can be observed that Eurocode 4 is in quite good agreement with the analysis results for CFT columns with normal-strength concrete ( $f'_c < 35\text{ MPa}$ ). However, significant conservative predictions of the axial resisting capacity are observed when the compressive strength of concrete is relatively high. Furthermore, there are only slight differences in the concentric axial strength of CFT between the predictions of Eurocode 4 and the unconfined case. This can be explained by the equation for the axial plastic resistance given by Eurocode 4 (see Eq. (13)). The plastic capacity is

represented as  $N_{pl,rk} = \eta_{a0}A_s f_y + (1+k)A_c f'_c$  where  $k = \eta_{a0} t f_y / D f'_c$ . Therefore, the proportions of the axial resisting capacity provided by the steel tube and the concrete are simply represented by the coefficients  $\eta_{c0}$  and  $k$ , respectively. While  $\eta_{a0}$  linearly increases from 0.915 to 0.96 as the strength of the concrete ranges from 25MPa to 75MPa, the coefficient  $k$  decreases dramatically from 0.15 to 0.01. Thus, the compressive strength increment of concrete due to confinement pressure is neglected as the strength of the unconfined case increases. However, this underestimation is not serious because the error is less than 10%. Meanwhile, the overestimations of Eurocode 4 are near the point of balanced eccentricity, but the error is also less than 10%.

## **7. Conclusions**

A one dimensional fiber beam finite element model to evaluate the behavior and ultimate resisting capacity of a circular CFT is proposed by adopting a proper material model for the confinement effect. The validity of the proposed numerical analysis model is established by comparing the analytical predictions with results from previous experimental studies about pure bending and eccentric compression cases. Moreover, the analysis result gives accurate estimations of both the behavior and the ultimate resisting capacity of CFT columns, while the analysis result using an unconfined material model significantly underestimates these values.

The ultimate resisting capacities predicted by the proposed numerical model and the design guidelines in Eurocode 4 are compared. The predictions by Eurocode 4 and the full plasticity interaction diagrams of CFT columns show good agreement with the analysis when normal-strength materials are used and when the column is relatively slender ( $kL/r=30$ ). In such a range, the modified version of Eurocode 4 successfully estimates the resisting capacities of CFT with variations of the depth-to-thickness ratio. In addition, overestimations are observed when high-strength concrete is combined with a normal-strength steel tube, and vice versa. Although rigorous analysis involves increased computational effort, it should be done for a proper design of such a column.

## **Acknowledgments**

This work was supported by the Innovations in Nuclear Power Technology of the Korea Institute of Energy Technology Evaluation and Planning (20101620100050) grant funded by the Korea government Ministry of Knowledge Economy and a grant (07High Tech A01) from the High-tech Urban Development Program funded by the Ministry of Land, Transportation and Maritime Affairs of the South Korean government.

## **References**

- Baig, M.N., Fan, J. and Nie, J. (2006), "Strength of Concrete Filled Steel Tubular Columns", *Tsinghua Science & Technology*, **11**(6), 657-666.
- Elchalakani, M., Zhao, X. and Grzebieta, R. (2001), "Concrete-filled circular steel tubes subjected to pure bending", *J. of Constr. Steel Res.*, **57**(11), 1141-1168.
- Elremaily, A. and Azizinamini, A. (2002), "Behavior and strength of circular concrete-filled tube columns",

- J. of Constr. Steel Res.*, **58**(12), 1567-1591.
- Eurocode4 (2004), *Design of composite steel and concrete structures part 2. General rules and rules for bridges*, Brussels.
- Fam, A., Qie, F.S. and Rizkalla, S. (2004), "Concrete-filled steel tubes subjected to axial compression and lateral cyclic loads", *J. of Struct. Eng.*, **130**(4), 631-640.
- Furlong, R.W. (1967), "Strength of steel-encased concrete beam columns", *J. of the Struct. Division, ASCE*, **93**(ST5), 113-124.
- Giakoumelis, G. and Lam, D. (2004), "Axial capacity of circular concrete-filled tube columns", *J. of Constr. Steel Res.*, **60**(7), 1049-1068.
- Hajjar, J.F. and Gourley, B.C. (1996), "Representation of concrete-filled steel tube cross-section strength", *J. of Struct. Eng.*, **122**(11), 1327-1336.
- Hatzigeorgiou, G. D. (2008), "Numerical model for the behavior and capacity of circular CFT columns, Part II: Verification and extension", *Eng. Struct.*, **30**(6), 1579-1589.
- Hu, H., Su, F. and Elchalakani, M. (2010), "Finite element analysis of CFT columns subjected to pure bending moment", *Steel. Compos. Struct.*, **10**(5), 415-428.
- Hu, H.T., Huang, C.S., Wu, M.H. and Wu, Y.M. (2003), "Nonlinear analysis of axially loaded concrete-filled tube columns with confinement effect", *J. of Struct. Eng., ASCE*, **129**(10), 1322-1329.
- Huang, F., Yu, X. and Chen, B. (2012), "The structural performance of axially loaded CFST columns under various loading conditions", *Steel. Compos. Struct.*, **13**(5), 351-471.
- Kwak, H.G. and Fillippou, F.C. (1990), *Finite element analysis of reinforced concrete structures under monotonic loads*, University of California at Berkeley, California.
- Kwak, H.G. and Kwak, J.H. (2010), "An improved design formula for a biaxially loaded slender RC column", *Eng. Struct.*, **32**(1), 226-237.
- Kwak, H.G. and Kwak, J.H. (2012), "Ultimate resisting capacity of axially loaded circular concrete-filled steel tube columns", *J. of the korea conc. inst.*, **24**(4), 423-433.
- Lakshmi, B. and Shanmugam, N. (2002), "Nonlinear analysis of in-filled steel-concrete composite columns", *J. of Struct. Eng.*, **128**(7), 922-933.
- Liang, Q.Q. and Fragomeni, S. (2009), "Nonlinear analysis of circular concrete-filled steel tubular short columns under axial loading", *J. of Constr. Steel Res.*, **65**(12), 2186-2196.
- Liu, G.Y., Yeh, Y.K., Tsai, K.C., Su, S.C. and Sun, W.L. (2003), *A Study on the behaviors of concrete-filled steel tubular beam - columns subjected to axial load and bending moment*, National Center for Research on Earthquake Engineering, Taipei.
- Mander, J.B., Priestley, M. J.N. and Park, R. (1988), "Theoretical Stress-Strain Model for Confined Concrete", *J. of Struct. Eng.*, **114**(8), 1804-1826.
- O'Shea, M.D. and Bridge, R.Q. (1998), "Tests on circular thin-walled steel tubes filled with medium and high strength concrete", *Australian civil engineering transactions*, **40**(1), 15-27.
- O'Shea, M.D. and Bridge, R.Q. (2000), "Design of circular thin-walled concrete filled steel tubes", *J. of Struct. Eng.*, **126**(11), 1295-1303.
- Richart, F.E., Brandtzaeg, A. and Brown, R.L. (1928), *A study of the failure of concrete under combined compressive stresses*, University of Illinois Engineering Experimental Station, Champaign, Ill.
- Sakino, K., Nakahara, H., Morino, S. and Nishiyama, I. (2004), "Behavior of centrally loaded concrete-filled steel-tube short columns", *J. of Struct. Eng.*, **130**(2), 180-188.
- Schneider, S. P. (1998), "Axially loaded concrete-filled steel tubes", *J. of Struct. Eng.*, **124**(10), 1125-1138.
- Susantha, K.A.S., Ge, H. and Usami, T. (2001), "Uniaxial stress-strain relationship of concrete confined by various shaped steel tubes", *Eng. Struct.*, **23**(10), 1331-1347.
- Wang, Q., Zhao, D. and Guan, P. (2004), "Experimental study on the strength and ductility of steel tubular columns filled with steel-reinforced concrete", *Eng. Struct.*, **26**(7), 907-915.